Motion and deposition of non-Brownian particles in upflow collectors

Vasilis N. Burganos, Christakis A. Paraskeva, Panagiotis D. Christofides, and Alkiviades C. Payatakes

Institute of Chemical Engineering and High Temperature Chemical Processes and Department of Chemical Engineering, University of Patras, Patras, Greece

The motion and deposition of suspended particles in upflow unit cells of sinusoidal shape are studied using a three-dimensional trajectory analysis. Particle stagnation and exclusion regions can develop at the entrance mouth of upflow cells, the extent and distribution of which depend on several parameters including particle size, flow rate, cell geometry, and cell inclination. It is found that the particle exclusion phenomenon can become very significant over a wide range of the preceding parameters and can have significant implications in network-based simulations of upflow or horizontal flow depth filtration. A new definition of the impacted fraction is introduced that is based on the particle *entrance velocity and the* actual *entrance region. Calculations of the deposition rate in sinusoidal collectors indicate that switching from a downflow to an upflow mode results in increased or decreased capture efficiency depending, chiefly, on the inclination of the unit collector.*

Keywords: particle deposition; trajectory analysis; upflow filtration; depth filtration

Introduction

Upflow and horizontal flow modes of depth filtration have recently proved attractive alternatives to traditional downward filtration of water and wastewater thanks to their high filtration efficiency, simplicity of installation and maintenance, and sustainability of operation. A notable practical application of such filtration modes is their use for the reduction of the solid matter concentration of highly turbid surface water to a level that will secure efficient operation and long service life of the main filtration system (e.g., conventional sand filter).[1] Upward and horizontal filtration processes occur also during enhanced oil recovery by flooding and are known to be responsible for considerable loss of the reservoir permeability.

Despite the great practical interest in such filtration processes, no relevant theoretical modeling or simulation attempt has appeared in the literature as yet. Hence, horizontal and upflow filtration process and equipment design is currently based on empirical or, at best, semiempirical models.[2] However, at least conceptually, most theoretical works on downward depth filtration can apply to horizontal and upflow filtration as well, subject to minor modifications. Particle trajectory-based simulators of depth filtration offer significant advantages over continuous models because they pay particular attention to the local flow details and the local physical chemistry of the particle-carrier-surface system. Typical up-to-date examples include the three-dimensional (3-D) network simulator by Burganos et al.,[3] the grain model by Vitthal and Sharma,[4] and the test particle approach by Imdakm and Sahimi.[5] Computation of particle trajectories in all these works involves evaluation of the main forces and torques acting on a test particle and monitoring of the particle motion by either integrating directly the particle trajectory equation or inverting the particle mobility tensor.

A practical problem that is encountered when particle motion simulators are used to simulate upflow or horizontal flow filtration is the following. Upflow deposition cells (not necessarily vertical) may contain areas where particles stagnate, or from which particles are excluded. This phenomenon is caused by the competitive action of the hydrodynamic and gravitational forces in upflow cells, and may become of primary

Address reprint requests to Dr. A. C. Payatakes at the Department of Chemical Engineering, University of Patras, GR 265 00, Patras, Greece
Received 10 May 1993; accepted 3 June 1993

significance depending on the local flow rate, the particle density and size, and the pore geometry and orientation. In addition to affecting the local deposition rate, this force interplay can create particle entrance regions at both pore ends, and complicate the particle trajectory calculations, the form of the population balance equation, and the pore-to-pore particle transition simulation. For instance, the probability of a particle that arrives at a pore intersection to enter a particular adjacent pore segment should be proportional to the local *particle-entrance rate* through the *actual* pore-entrance region, and not to the local flow rate as is the invariable assumption in network models of downflow filtration.[3,5,13–16] It is obvious, however, that this particle exclusion phenomenon can appear only when working with non-Brownian particles, because Brownian particles practically follow the carrier-phase streamlines.

In the present work an investigation of the particle entrance, stagnation, and exclusion regions in upflow deposition cells of sinusoidal shape, used to simulate the pore space of unconsolidated materials, is made through computation of critical particle trajectories. Hydrodynamic forces and torques including the effects of particle-collector hydrodynamic interaction, gravity, and surface forces are taken into account in our computations. The effects of flow rate, particle size, and pore orientation on the extent of the particle exclusion phenomenon and on the deposition rate are quantified, and their potential implications on the performance and predictions of deep bed filtration simulators are discussed. Finally, residence time distribution calculations for escapee particles through upflow and downflow collectors are presented, and real travel times for various particle entrance positions are compared for the two flow modes.

Notation

A_i, B_i, D_i	variables used for the description of the undisturbed flow in the immediate vicinity of the wall of a unit cell of the i^{th} type
A_i^+, B_i^+, D_i^+	dimensionless variables
a_p	particle radius, μm
C_0	entrance concentration of the suspension
$\mathbf{F}_D$	hydrodynamic force exerted on the suspended particle, N
$\mathbf{F}_E$	electrokinetic force exerted on the suspended particle, N
$\mathbf{F}_G$	gravitational force exerted on the suspended particle, N
$\mathbf{F}_L^{ret}$	London force exerted on the suspended particle (corrected for the retardation effect), N
F_{Gz}, F_{Dz}	axial components of $\mathbf{F}_G$ and $\mathbf{F}_D$, respectively
F_4, F_5, F_6	universal functions
f_y^m	universal function
H	Hamaker constant, J
h_0	length of the unit cell, μm
N_{DL}	double-layer parameter (dimensionless)
N_{E1}, N_{E2}	first and second dimensionless electrokinetic group
N_G	dimensionless gravitational group
N_{Lo}	London parameter (dimensionless)
N_{RS}	relative size group (dimensionless)
$\mathbf{T}_D$	hydrodynamic torque
U_∞	$2(\rho_p - \rho)a_p^2 g/9\mu$, limiting fall velocity
u_z	magnitude of the axial velocity of the particle, mm s^{-1}
r	radial cylindrical coordinate, μm
$R_0(\theta)$	radial coordinate of limiting particle trajectory
R^*	critical radial coordinate for limiting particle entrance
R_1, R_2	mouth radii of the unit cell, μm
$\mathbf{v}$	fluid velocity in the absence of suspended particles (undisturbed fluid velocity), m s^{-1}
v_z, v_r, v_θ	z, r, θ components of $\mathbf{v}$
v_0	mean entrance velocity of the fluid, mm s^{-1}
z	axial cylindrical coordinate

Greek letters

α	angle formed by the z-axis and the tangent on the wall of a sinusoidal tube, degrees
$\alpha_{s,p}$	retardation factor for London, the force between a sphere and a plate with semi-infinite thickness
Γ_1, Γ_2, Γ_3	functions defined in the appendix
δ	separation between spherical particle and unit cell wall
δ^+	δ/a_p, dimensionless separation
η	number fraction of particles coming to collision with the wall
ζ_1, ζ_2	intrinsic coordinates used in trajectory calculation
ζ_1^+, ζ_2^+	defined as ζ_1/a_p, ζ_2/a_p, respectively
θ	angular cylindrical coordinate, degrees
κ	double-layer reciprocal thickness, m^{-1}
ϕ	angle formed by the z-axis of a unit cell and the horizontal, degrees
ψ_{01}, ψ_{02}	surface potential of suspended particle and grain, respectively, mV

Particle trajectory method and identification of particle motion regions

Consider the case of upward creeping flow of a dilute suspension of non-Brownian particles through a sinusoidal unit cell. We use the term *upflow cell* to denote a pore or a unit cell of a pore network in which the axial component of the mean fluid velocity points upward. A suspended non-Brownian particle translates under the action of gravity ($\mathbf{F}_G$), the hydrodynamic force ($\mathbf{F}_D$), the London-van der Waals force ($\mathbf{F}_L^{ret}$), and the electrokinetic force ($\mathbf{F}_E$), and it rotates under the action of the hydrodynamic torque ($\mathbf{T}_D$) that develops close to the pore wall. Neglecting particle inertia and interparticle interactions (which are two well-established simplifications for typical depth filtration systems) the linear and angular momentum equations become

$$\mathbf{F}_G + \mathbf{F}_D + \mathbf{F}_L^{ret} + \mathbf{F}_E = 0 \tag{1}$$

$$\mathbf{T}_D = 0 \tag{2}$$

and can be used to derive the particle trajectory equations in the 3-D space of a unit cell. The final form of these equations, derived by Paraskeva et al.,[6] is given in the appendix. The required flow field solution is obtained using the collocation procedure described by Tilton and Payatakes,[7] the particle-wall hydrodynamic interactions have been included using the hydrodynamic universal functions provided in the literature,[8–11] and the retardation effect has been taken into account in the calculation of the London force following the work of Payatakes et al.[12]

Thanks to the sinusoidal shape of the pore wall, the axial (z-) component of the particle velocity at the pore entrance is obtained from the simple equation

$$F_{Gz} + F_{Dz} = 0 \tag{3}$$

This implies that a particle can enter, or fail to enter, a pore depending solely on the competition between gravity and the drag force, irrespective of the surface forces.

Figure 1 shows the various regions and modes of particle motion that may develop in a vertical (*a*) and an inclined (*b*) upflow unit cell. Note the existence of a locus of particle stagnation positions in the interior of the vertical unit cell that reduces to a circle of radius R^* on the entrance plane. Three distinct regions are observed in the vertical cell case. Particles with entrance radial coordinate, r, satisfying $0 < r < R^*$ manage to enter the unit cell, whereas particles in $R^* < r < R_1 - a_p$ (R_1: pore mouth radius; a_p: particle radius) fail to enter the pore space. Once entrance to the unit cell is accomplished, the trajectory of a test particle is computed using the two-dimensional particle trajectory equation as this results from the full force and torque balance equations (Equations 1 and 2) (any particle trajectory in a vertical axisymmetric cell lies on a single plane that contains the axis of the cell). The trajectory of a particle that enters a vertical unit cell at virtually nil velocity is depicted in *Figure 1a*. Note that the particle acquires progressively higher velocity while in the lower half of the cell, as indicated by its approaching the pore axis faster than the corresponding streamline. This phenomenon is exactly inversed in the upper half of the cell leading to escape of the particle. Using the same reasoning, it is clear that particles in the region $R^* < r < R_1 - a_p$ on the upper mouth plane (arriving there from neighboring unit cells during a pore network simulation) will enter the unit cell moving downward. For the parameter values used in *Figure 1a* these particles will finally deposit on the pore surface. However, it may happen that such particles move across the unit cell and escape from the lower mouth. This double-entrance double-exit phenomenon is enhanced by low flow rate, large particle size, and large constriction-to-mouth size ratio.

Integration of the full 3-D particle trajectory equations is required to monitor the 3-D motion of particles in inclined cells. *Figures 1b* and *2a* show that inclined upflow cells behave in a substantially different manner from that of vertical cells. *Figure 1b* displays trajectories of particles that enter through the bottom mouth and, after following a short course in the interior of the pore, exit through the same face at positions near the pore wall where very low fluid velocities develop. If structure periodicity in the axial direction is assumed, it may happen that certain entrance positions lead to trajectories that cross the exit face of the cell and, after a short course in the adjacent unit cell, reenter the original cell. Because of the axial symmetry of the flow field and the fact that the radial component of the fluid velocity vanishes at the maximal cross-sections of sinusoidal tubes, the locus of stagnation points on the entrance face is a circle for any cell inclination (see, e.g., *Figure 2a*). However, this is not the case for the locus of particle entrance positions that lead to limiting capture at the edge of the exit mouth, which is a strongly r-dependent curve. It is important to note that the locus of entrance positions that lead to entry into the cell and capture is the shaded area contained between these two loci (*Figure 2a*). For the sake of comparison, the corresponding regions of particle entrance positions that lead to deposition in the same unit cell but with inversed direction of flow (downflow mode) are shown in *Figure 2b*. The downflow case is free of particle stagnation phenomena. Particles can enter through almost the entire mouth of the cell (except for the indiscernible region $R_1 - a_p < r < R_1$ from which the center of the particle is excluded for reasons of steric hindrance). Hence, the region of initiation of capture trajectories in the downflow case extends, practically, to the edge of the cell mouth in contrast to that in the upflow case (compare *Figures 2b* and *2a*).

The existence of pore mouth regions that exclude particle entry suggests a new definition of the impacted fraction in an upflow unit cell which, in addition, makes use of the *particle* entrance velocity in place of the previously used *fluid* velocity.

$$\eta = \frac{\int_{-\pi}^{\pi} \int_{R_{01}(\theta)}^{R_{02}(\theta)} u_z(r, \theta) C_0 r \, dr \, d\theta}{\int_{-\pi}^{\pi} \int_{0}^{R^*} u_z(r, \theta) C_0 r \, dr \, d\theta} \tag{4}$$

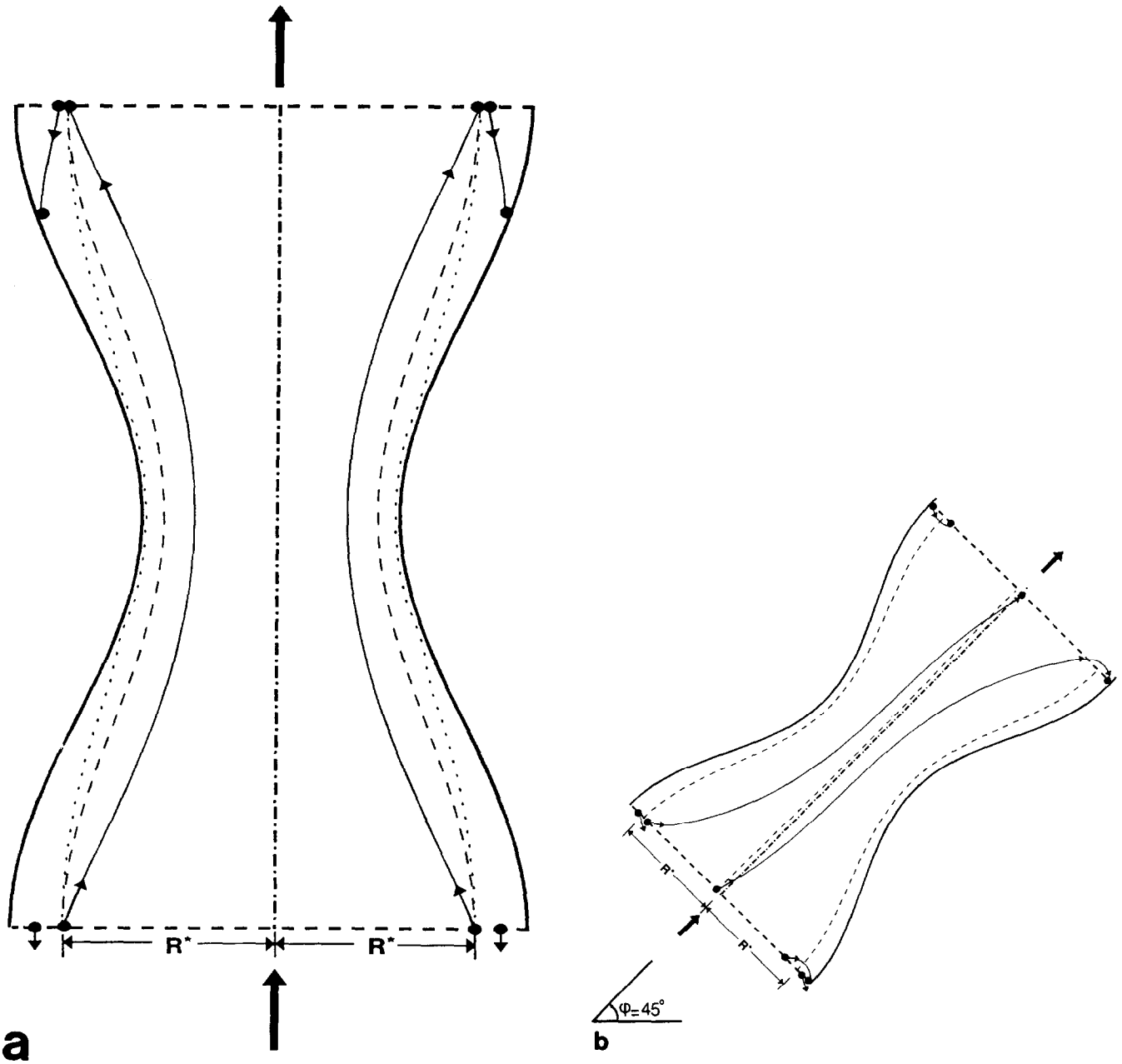

Figure 1 Locus of particle stagnation points (· · · ·), limiting capture and escape trajectories (——), and corresponding streamlines (– – –) in (a) vertical and (b) inclined upflow cells. a_p = 5 μm; v_0 = 0.2 mm s^{-1}. All other parameter values from *Table 1*.

In Equation 4, C_0 is the particle concentration at the entrance face, $u_z(r, \theta)$ is the magnitude of the axial component of the particle entrance velocity (calculated from the force balance, Equation 3), and $R_{01}(\theta)$, $R_{02}(\theta)$ are the θ-dependent minimal and maximal radial coordinates, respectively, of entrance positions that lead to limiting capture trajectories. Hence, the impacted fraction, η, is the number fraction of particles that actually enter the unit cell per unit time and come to collision with the wall.

Subsequently, we present a collection of the most important numerical results of critical entrance position and impacted fraction calculations for upflow cells using as parameters the particle size, the mean entrance velocity, and the pore inclination. We also compare the particle collection efficiency of upflow and downflow unit cells at various inclinations for different constriction-to-mouth size ratios.

Results and discussion

The dependence of the critical radial position for limiting particle entrance into a vertical upflow cell on the mean entrance velocity for various particle sizes is

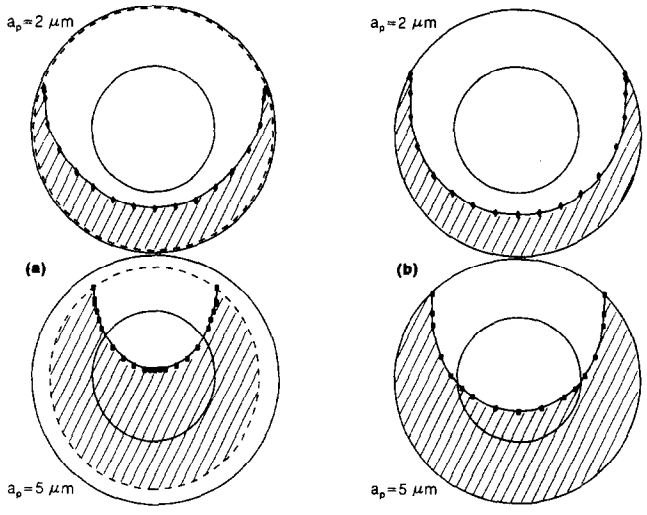

Figure 2 Loci of particle stagnation positions (dashed circles) and of entrance positions that lead to limiting capture (marked points) in an inclined (45°) unit collector under (a) upflow and (b) downflow conditions. *Top*, a_p = 2 μm; *bottom*, a_p = 5 μm. v_0 = 0.2 mm s^{-1}. All other parameter values from *Table 1*.

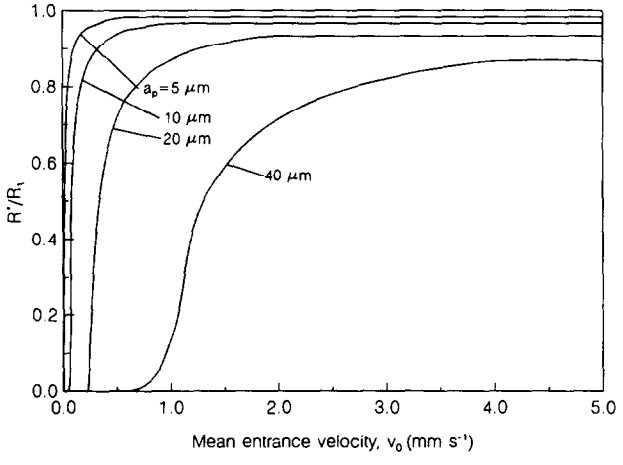

Figure 3 Critical radial coordinate for limiting particle entrance vs. mean fluid entrance velocity in a vertical upflow unit cell. Variation with the particle size. All other parameter values from *Table 1*.

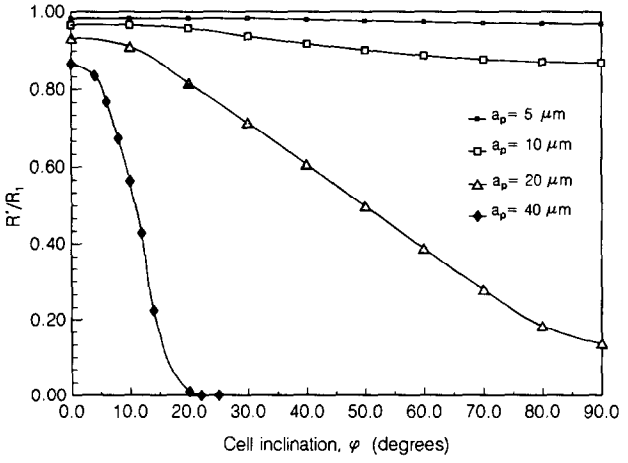

Figure 4 Dependence of the critical radial distance on the cell inclination with respect to the horizontal in an upflow cell. Variation with the particle size. Mean fluid entrance velocity v_0 = 0.25 mm s^{-1}. All other parameter values from *Table 1*.

Table 1 Parameter values used in the trajectory calculations

r_c = 150 μm	N_{Ret} = 314.2
$R_1 = R_2$ = 300 μm	N_G = 0.02258
h_0 = 1,000 μm	N_{E1} = 53.10
ψ_{01} = −30 mV	N_{DL} = 1400
ψ_{02} = −8 mV	N_{Lo} = 5.83 10^{-5}
κ = 2.8 10^8 m^{-1}	N_{RS} = 5 10^{-3}
H = 5 10^{-20} J	

shown in *Figure 3*. At very low flow rates the particle exclusion region extends over the entire entrance mouth ($R^* \rightarrow 0$). As the mean fluid velocity increases, the particle entrance region increases quickly at a rate that also increases with decreasing particle size. At sufficiently high fluid velocities particles can enter the pore through the entire entrance mouth; the critical radial coordinate of the particle center in that case is $R_1 - a_p$.

Horizontal unit cells are free of this particle exclusion phenomenon, because gravity acts perpendicularly to the drag force at the entrance mouth. However, as the unit cell becomes oblique and conducts the suspension in the upflow mode, the actual entrance region decreases drastically, as shown in *Figure 4*, except for the case of very small particles (say, $a_p \leq 10$ μm). At a fluid entrance velocity of 0.25 mm s^{-1}, for instance, no 40-μm particle can enter unit cells of the particular geometry considered here (see *Table 1*) that are inclined more than 20° from the horizontal, whereas 20-μm particles enter a vertical upflow cell only through a very narrow region near the pore axis. In a pore network simulation of upflow and horizontal flow filtration, therefore, it is expected that large particles can enter the filter only through a relatively small number of unit cells and have a very low probability of penetrating into large depths.

The variation of the impacted fraction in upflow unit cells with the cell inclination is presented in *Figure 5* for two values of the constriction-to-mouth size ratio (r_c = 90 μm and 150 μm, R_1 = 300 μm) and compared with that in downflow cells of the same inclination and for the same flow rate. The impacted fraction in upflow cells is higher than that in downflow cells, over a wide range of cell inclinations, but drops to very small values in a narrow range close to the vertical orientation. Extensive trajectory computations over a wide range of constriction-to-mouth size ratios, particle sizes, and flow rates showed that particle capture is practically

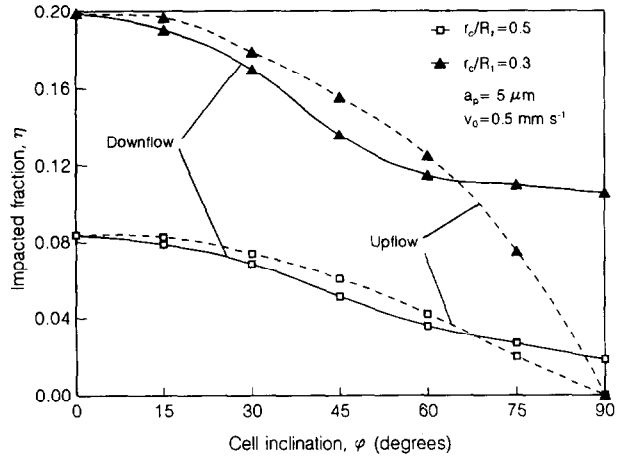

Figure 5 Impacted fraction vs. cell inclination in upflow and downflow unit cells for two values of the constriction-to-mouth size ratio. All other parameter values from *Table 1*.

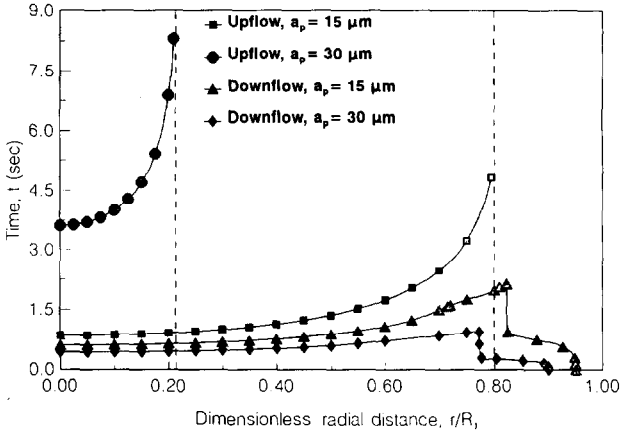

Figure 6 Travel time vs. radial coordinate of entrance position in upflow and downflow vertical unit cells. Variation with the particle size. Mean fluid entrance velocity $v_0 = 0.5$ mm s^{-1}. All other parameter values from *Table 1*.

impossible in symmetric vertical upflow cells. The reason for this negligible collection efficiency is that in vertical upflow cells the particle is driven by the gravitational and drag forces away from the wall, and, hence, it is kept away from the action of the short-ranged attractive surface forces that could potentially lead it to capture. It seems that the impacted fraction in vertical upflow cells can attain a finite value only in the case of small particles entering the pore at positions very close to the wall within the range of action of the London force. In this particular case the value of the impacted fraction is negligibly small.

It is also very interesting to investigate the effect of the choice of upflow or downflow operation on the travel time (residence time or passage time) of suspended particles through constricted unit cells. The results of this study can be directly used in dynamic simulations of depth filtration, where timing of the sequential and simultaneous particle deposition events is of primary importance for the determination of the local deposit morphology, of the temporal evolution of the permeability profile across the filter, and of the effluent composition.

Figure 6 shows the dependence of the travel time of particles that either escape through or deposit in upflow and downflow, vertical sinusoidal unit cells. (Calculation of the travel time is straightforward thanks to the omission of inertial forces from the particle trajectory equations and to the assumption of no reentrainment.) The travel time of escaping particles (passage time) is larger in upflow cells than in downflow ones of the same geometry and for the same flow rate. This time difference increases with increasing radial distance of the incoming particles at the entrance mouth and with increasing particle size. As the critical radial distance in upflow cells is approached, the particle entrance velocity tends to very small values and the time required by the particles to proceed a few particle diameters into the pore becomes quite large.

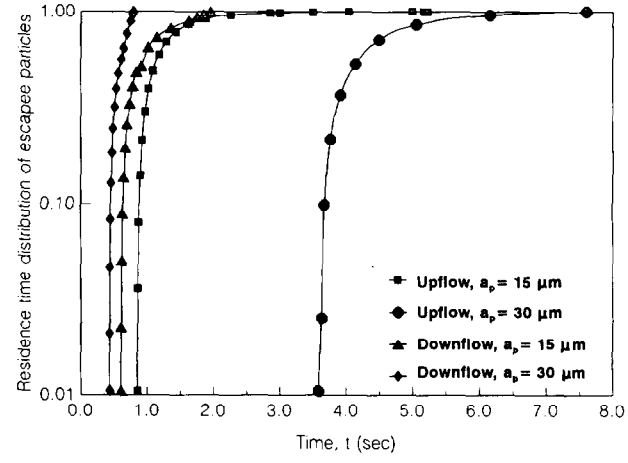

Figure 7 Residence time distribution of escaping particles in upflow and downflow vertical unit cells for two particle sizes. Mean fluid entrance velocity $v_0 = 0.5$ mm s^{-1}. All other parameter values from *Table 1*.

This explains the rapid increase in the passage time observed in *Figure 6*. A different situation is encountered in downflow cells. The travel time increases with increasing radial distance at the entrance mouth and reaches a (finite) maximal value where the radial distance corresponds to limiting capture (i.e., capture at the edge of the exit mouth). Particle trajectories that are initiated at radial distances larger than this critical value lead to capture at positions closer to the entrance face and require progressively smaller travel times. The sharp decrease in the travel time curve immediately past the maximum reflects the very low capture efficiency of the upper half of vertical downflow cells already quantified in terms of the local deposition rate in Burganos et al.[13]

The residence time distribution of escapee particles in upflow and downflow vertical cells is shown in *Figure 7* for two particles sizes in the form $J(t)$ vs. t, where

$J(t)$ is the number fraction of escapee particles with residence (passage) time less than t. The upflow case curves approach unity asymptotically. On the contrary, the residence time distribution function in the downflow cases becomes unity at finite time values, which correspond to limiting captures.

Conclusions and further remarks

A 3-D particle trajectory analysis of suspension flow and particle deposition in vertical and oblique upflow unit cells of sinusoidal shape was developed. Depending on the interplay of gravity and hydrodynamic forces, stagnation and particle exclusion regions can develop at the entrance face of the pore. The critical radial coordinate for limiting particle entrance into the pore space was found to decrease rapidly with increasing particle size, decreasing flow rate, and increasing inclination with respect to the horizontal. Comparison of impacted fraction values in upflow and downflow unit cells showed that upflow cells have increased collection efficiency at small and medium pore inclination angles. However, vertical and nearly vertical unit cells present negligible particle capture efficiency because of the fact that the actual particle entrance region consists of positions that are well outside the range of action of the attractive London force.

The immediate implications of the results and conclusions of this work on network simulations of particle deposition in porous materials are the following: Each upflow unit cell of the network must be investigated separately for the identification of possible particle stagnation and exclusion regions. Account must be made for particles that arrive at nodes that are adjacent to upflow cells. If the node is at the entrance mouth of an upflow cell, particles can enter through the allowed entrance region only, and not through the entire mouth as happens with horizontal and downflow cells. If the node is located at the exit mouth of an upflow cell, arriving particles can enter the upflow cell (moving downward) at positions near the pore wall where the fluid velocity is sufficiently small and assume a trajectory that can either lead to deposition on the wall or to escape through the lower mouth of the cell. The deposition rate in such double-entrance upflow cells must be calculated in a manner that takes into account deposition of particles traveling both upstream and downstream. Moreover, the deposition rate in every unit cell of the network must be calculated using the *particle entrance velocity* in place of the fluid entrance velocity employed in previous models and simulations. Because our calculations indicate that vertical upflow cells have negligible collection efficiency, it is expected that cubic networks of sinusoidal pores having one main direction aligned with the macroscopic flow (also gravity) direction will prove less efficient collectors, if operated in the upflow mode rather than the downflow mode. However, if none of the main directions of the network is vertical or nearly vertical, upflow operation is expected to yield a considerably higher particle removal efficiency than that obtained during downflow operation. Verification and quantification of these predictions can only be provided by a thorough 3-D network analysis of upflow, downflow, and horizontal flow filtration that will be presented in a future publication.

In closing, it should be stressed that the particle trajectory analysis used in this work permits direct evaluation of passage and capture times in upflow and downflow cells. These results, combined with residence time distribution results such as those presented here, can be used to form a very useful database that could decisively simplify network-based simulations of hydrodynamic chromatography and transient filtration processes.

Acknowledgments

This work was supported by the EC Programme PRD Grant 14EIXH2, and by the Institute of Chemical Engineering and High Temperature Chemical Processes.

References

1. Wegelin, M., Schertenleib, R. and Boller, M. The decade of roughing filters—development of a rural water-treatment process for developing countries. *J. Water SRT—Aqua* 1991, **40**, 304
2. Wegelin, M., Boller, M. and Schertenleib, R. Particle removal by horizontal-flow roughing filtration. *J. Water SRT—Aqua* 1987, **36**, 80
3. Burganos, V.N., Paraskeva, C.A. and Payatakes, A.C. Three-dimensional trajectory analysis and network simulation of deep bed filtration. *J. Colloid Interface Sci.* 1992, **148**, 167
4. Vitthal, S. and Sharma, M.M. A stokesian dynamics model for particle deposition and bridging in granular media. *J. Colloid Interface Sci.* 1992, **153**, 314
5. Imdakm, A.O. and Sahimi, M. Computer simulation of particle transport processes in flow through porous media. *Chem. Eng. Sci.* 1991, **46**, 1977
6. Paraskeva, C.A., Burganos, V.N. and Payatakes, A.C. Three-dimensional trajectory analysis of particle deposition in constricted tubes. *Chem. Eng. Comm.* 1991, **108**, 23
7. Tilton, J.N. and Payatakes, A.C. Collocation solution of creeping newtonian flow through sinusoidal tubes: A correction. *AIChE J.* 1984, **30**, 1016
8. Brenner, H. The slow motion of a sphere through a viscous fluid towards a plane surface. *Chem. Eng. Sci.* 1961, **16**, 242
9. Goren, S.L. and O'Neill, M.E. On the hydrodynamic resistance to a particle of a dilute suspension when in the neighbourhood of a large obstacle. *Chem. Eng. Sci.* 1971, **26**, 325
10. O'Neill, M.E. A slow motion of viscous liquid caused by a slowly moving solid sphere. *Mathematica* 1964, **11**, 67
11. Goldman, A.J., Cox, R.G. and Brenner, H. Slow viscous motion of a sphere parallel to a plane wall. *Chem. Eng. Sci.* 1967, **22**, 637
12. Payatakes, A.C., Tien, C. and Turian, R.M. Trajectory calculation of particle deposition in deep bed filtration: I. Model formulation. *AIChE J.* 1974, **20**, 889
13. Burganos, V.N., Paraskeva, C.A. and Payatakes, A.C. Parametric study of particle deposition in sinusoidal pores of arbitrary orientation. *J. Colloid Interface Sci.* 1993, **158**, 466
14. Imdakm, A.O. and Sahimi, M. Transport of large particles in flow through porous media. *Phys. Rev. A* 1987, **36**, 5304
15. Rege, S.D. and Fogler, H.S. Network model for straining dominated particle entrapment in porous media. *Chem. Eng. Sci.* 1987, **42**, 1553
16. Rege, S.D. and Fogler, H.S. A network model for deep bed filtration of solid particles and emulsion drops. *AIChE J.* 1988, **34**, 1761

Appendix: Particle trajectory equations

The 3-D particle trajectory equations in terms of the intrinsic coordinates are

$$\frac{d\zeta_2^+}{d\zeta_1^+} = \frac{-A_i^+ \zeta_2^{+2} f_y^m - N_G \Gamma_2 + N_{E1}(N_{E2} - e^{-N_{DL}\delta^+}) \dfrac{e^{-N_{DL}\delta^+}}{(1 - e^{-2N_{DL}\delta^+})} - \dfrac{N_{Lo}\alpha_{s,p}(\delta^+; N_{Re1})}{\delta^{+2}(2 + \delta^+)^2}}{B_i^+ \zeta_2^+ F_4 + D_i^+ \zeta_2^{+2} F_5 + N_G F_6 \Gamma_1}$$

$$\frac{d\theta}{d\zeta_1^+} = -\frac{1}{r} \frac{F_6 N_G \Gamma_3}{B_i^+ \zeta_2^+ F_4 + D_i^+ \zeta_2^{+2} F_5 - N_G F_6 \Gamma_1}$$

where $\zeta_1^+ = \zeta_1/a_p$ and $\zeta_2^+ = \zeta_2/a_p$ and

$$\Gamma_1 = -\cos\phi \cos\theta \sin\alpha + \sin\phi \cos\alpha$$

$$\Gamma_2 = -\cos\phi \cos\theta \cos\alpha - \sin\phi \sin\alpha$$

$$\Gamma_3 = \cos\phi \sin\theta$$

When the particle is sufficiently far from the wall, the following trajectory equations, in terms of the polar coordinates, are used:

$$\frac{dr}{dz} = -\frac{U_\infty \cos\phi \sin\theta + v_r}{-U_\infty \sin\phi + v_z}$$

$$\frac{d\theta}{dz} = \frac{-U_\infty \cos\phi \cos\theta}{r(-U_\infty \sin\phi + v_z)}$$